Construction and Building Materials 223 (2019) 1095–1105

Contents lists available at ScienceDirect

Construction and Building Materials

journal homepage: www.elsevier.com/locate/conbuildmat

Effect of double hooked-end steel fiber on early-age cracking potential of high strength concrete in restrained ring specimens

Dejian Shen [a,b,c,*], Jiacheng Kang [a,b], Xijun Yi [a,b], Liukun Zhou [a,b], Xiang Shi [a,b]

[a] College of Civil and Transportation Engineering, Hohai Univ., No. 1, Xikang Rd., Nanjing 210098, China
[b] Jiangsu Engineering Research Center of Crack Control in Concrete, No.1, Xikang Rd., Nanjing 210098, China
[c] Nanjing Engineering Research Center for Prefabricated Construction, No.1, Xikang Rd., Nanjing 210098, China

HIGHLIGHTS

- Cracking potential of steel fiber reinforced concrete was studied by ring test.
- Residual stress or relaxed stress decreased with increasing amount of steel fiber.
- Free shrinkage or stress rate decreased with increasing amount of steel fiber.
- Cracking potential decreased with increasing amount of steel fiber.

ARTICLE INFO

Article history:
Received 16 September 2018
Received in revised form 26 July 2019
Accepted 29 July 2019
Available online 8 August 2019

Keywords:
High strength concrete
Early age
Steel fiber
Cracking potential
Ring test
Stress relaxation

ABSTRACT

High strength concrete (HSC) suffers significant shrinkage in response to low water-to-cement (w/c) ratio and high self-desiccation at early age. Cracking may occur when the residual tensile stress is over the tensile strength of HSC. Double hooked-end steel fiber can reduce the shrinkage and the cracking potential of HSC effectively. Investigations on cracking potential of early-age HSC reinforced with double hooked-end steel fiber by utilizing ring test remain lacking. Therefore, ring tests for four HSC mixtures with different amounts of double hooked-end steel fiber of 0%, 0.12%, 0.24%, and 0.36% were conducted in the present study. The analysis of experimental results indicated that (1) the steel ring strain decreased with increasing amount of double hooked-end steel fiber; (2) the residual stress or relaxed stress of HSC decreased with increasing amount of double hooked-end steel fiber; (3) the free shrinkage or stress rate of HSC decreased with increasing amount of double hooked-end steel fiber; (4) the cracking potential of HSC decreased with increasing amount of double hooked-end steel fiber. At the age of 21.25 d after casting, the cracking potential parameter was 0.875, 0.561, 0.440, and 0.329, which decreased by 35.9%, 49.7%, and 62.4% when the amount of double hooked-end steel fiber increased from 0% to 0.12%, 0.24%, and 0.36%, respectively.

1. Introduction

High strength concrete (HSC) is utilized widely for its superiority. HSC with lower water-to-cement (w/c) ratios possesses several advantages compared with normal strength concrete, such as higher workability, higher strength, higher durability, and lower permeability [1–5]. However, low w/c ratios bring about high self-desiccation [6–8], which leads to significant autogenous shrinkage and increases the cracking potential of early-age HSC under restrained condition [9]. Early age is an important period during the lifetime of concrete [10]. Early-age cracking offers accesses for water and aggressive chemical ions [11], which not only weakens the bearing capacity of concrete structures but also reduces service life and durability of concrete structures [12,13]. The addition of steel fiber improves the mechanical properties and reduces cracking potential of concrete [14–18]. Double hooked-end steel fiber is better anchored in HSC compared with ordinary steel fiber [19–21]. The double hooked-end steel fiber is added to concrete to restrain the development of microcracking and reduce cracking potential of HSC at early age [22–24]. Investigations on cracking potential of concrete reinforced with steel fiber have been conducted [14,17,22]. However, investigations on influence of double hooked-end steel fiber on HSC remain lacking. Therefore,

* Corresponding author at: College of Civil and Transportation Engineering, Hohai Univ., No. 1, Xikang Rd., Nanjing 210098, China.
E-mail address: shendjn@163.com (D. Shen).

https://doi.org/10.1016/j.conbuildmat.2019.07.319
0950-0618/

investigations on the cracking potential of double hooked-end steel fiber reinforced HSC are necessary.

Ring test is normally utilized to estimate cracking potential of early-age concrete [12,25–28]. Tensile stress occurs in concrete ring specimens when the shrinkage is under restrained condition [29]. The shrinkage behavior and cracking potential of concrete under restrained condition is evaluated by utilizing ring test, as recommended by ASTM C1581 [30] and AASHTO [31]. Shrinkage is divided into two types: drying shrinkage and autogenous shrinkage [32,33]. Water evaporation, which leads to drying shrinkage, happens when the humidity inside concrete is higher than the environmental humidity [34,35]. Autogenous shrinkage occurs when cement hydration leads to moisture loss [12,36]. The results show that steel fiber can reduce shrinkage of plain concrete effectively [32,37,38]. However, investigations on influence of double hooked-end steel fiber on shrinkage of HSC at early age remain lacking. Therefore, investigations on shrinkage of HSC reinforced with double hooked-end steel fiber by utilizing ring test are necessary to understand the cracking mechanism of HSC better.

The cracking potential of concrete is also affected by stress relaxation [12,39,40]. The creep-related stress relaxation is an important factor for shrinkage analysis and early-age cracking potential evaluation of concrete [29,40–42]. Creep can significantly prevent cracking caused by shrinkage and thermal deformations in structures at early age and partly relieve the induced stresses [12,36]. Investigations on tensile creep of concrete have been conducted [42,43]. However, investigations on influence of double hooked-end steel fiber on creep-related stress relaxation of HSC remain lacking. Therefore, investigations on stress relaxation of HSC reinforced with double hooked-end steel fiber by utilizing ring test are necessary.

Investigations on mechanical properties of HSC reinforced with steel fiber have been conducted [22,44–48]. However, investigations on cracking potential of HSC reinforced with double hooked-end steel fiber at early age remain lacking. Therefore, investigations on steel ring strain, residual stress, free shrinkage, stress rate, stress relaxation, and cracking potential of HSC reinforced with double hooked-end steel fiber by utilizing ring test were conducted in the present study.

2. Experimental program

2.1. Mix proportions and materials

Four HSC mixtures utilized in the present study had the same w/c ratio of 0.32. Mixtures SF00, SF12, SF24, and SF36 were the HSC with steel fiber volume fraction of 0%, 0.12%, 0.24%, and 0.36%, respectively. The mix proportions of SF00, SF12, SF24, and SF36 are depicted in Table 1. The coarse aggregate in mixtures SF12, SF24, and SF36 was partially substituted with double hooked-end steel fiber, as reported in [45].

Portland Cement (P•II 52.5R) with the Blaine fineness of 375 m^2/kg was utilized in the present study according to Chinese National Standard GB 175–2007/XGI-2009 [49] and ASTM C150 [50]. The fine aggregate was nature river sand with fineness modulus of 2.1. The coarse aggregate was crushed limestone with the maximum size of 25 mm. The photograph of double hooked-end steel fiber utilized in the present study is depicted in Fig. 1. A kind of liquid polycarboxylate-based superplasticizer was utilized to achieve similar workability for four HSC mixtures. Tap water was utilized in four HSC mixtures for casting. Results of slumps were 165, 153, 142, and 131 mm for mixtures SF00, SF12, SF24, and SF36, respectively.

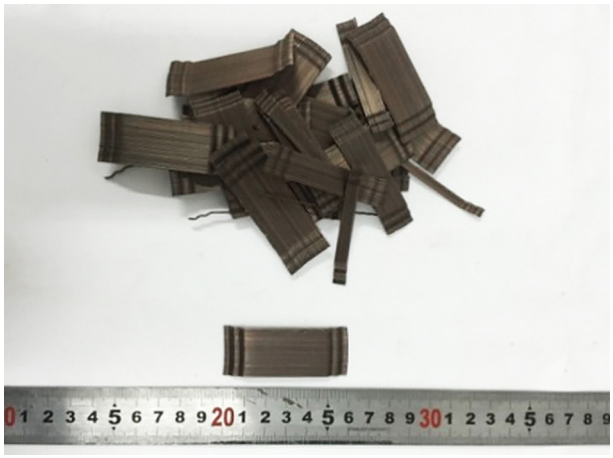

Fig. 1. Photograph of double hooked-end steel fiber.

2.2. Ring test

Fig. 2(a) and (b) depict the ring specimen geometry in detail with top view and cross view, respectively. The dimensions of inner (R_{IS}) and outer (R_{OS}) radius of the steel ring were 127.5 and 162.5 mm, respectively; the dimensions of inner (R_{IC}) and outer (R_{OC}) radius of the concrete ring were 162.5 and 262.5 mm, respectively. The steel rings utilized in the present study were all 100 mm tall. Eight strain gauges were utilized to determine the steel ring strain, ε_{st}, of each specimen continuously, as reported in [38,39]. The strain gauges were attached at the mid-height of the inner surface of the steel ring, as depicted in Fig. 2(b). The measurement of the steel ring strain started after casting. The steel ring strains were recorded at an interval of 30 min until the concrete cracked, as reported in [26,38,51]. Fig. 3 depicts the restrained ring test specimens in practice.

One concrete ring specimen was cast for each HSC mixture. After casting, the ring specimens were sealed with vinyl and aluminum tape on top surfaces immediately to prevent sudden drying. The specimens were cured at a constant temperature (23 ± 1) and relative humidity (60 ± 5%), as reported in [39]. The outer ring was taken off after 1 d of curing. Circumferential drying condition was provided according to the ASTM C1581 [30] and

Table 1
Mix proportions of concrete.

Mixture composition	SF00	SF12	SF24	SF36
Water (kg/m^3)	153.6	153.6	153.6	153.6
Cement (kg/m^3)	480	480	480	480
Fine aggregate (kg/m^3)	690	690	690	690
Coarse aggregate (kg/m^3)	1127.00	1123.32	1119.63	1115.95
Superplasticizer (kg/m^3)	3.84	3.84	3.84	3.84
Steel fiber (kg/m^3)	0	9.42	18.84	28.26
Steel fiber volume fraction (%)	0	0.12	0.24	0.36

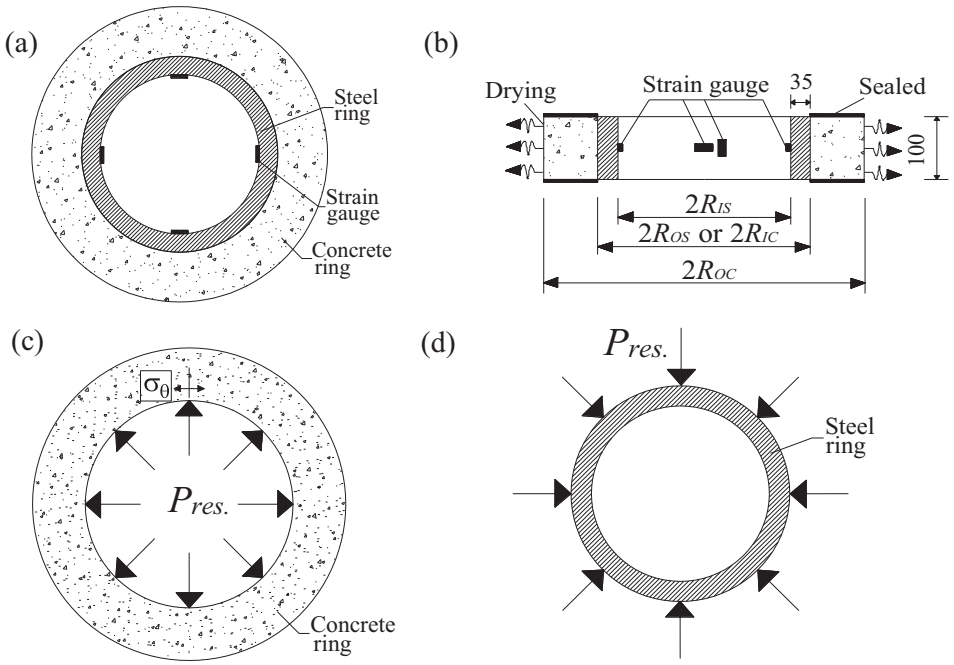

Fig. 2. Geometry of ring specimen: (a) Top view; (b) Cross view; (c) Concrete ring under surface pressure; (d) Steel ring under surface pressure (all units in mm).

AASHTO [31] to ensure that water evaporation was along the height of outer surface of concrete ring.

2.3. Free shrinkage measurements

The prismatic specimens with the size of 550 mm × 100 mm × 100 mm were tested to determine free shrinkage strain of HSC according to Chinese Standard GB/T 50082–2009 [52]. The restrained conditions of prismatic and ring specimens were different. However, the prismatic and ring specimens with an equal volume-to-surface area ratio are considered to have same free shrinkage [53]. Prismatic specimens were sealed partially with vinyl (i.e. 178 mm long from the ends) after demoulding to reach the target volume-to-surface area ratio, $V/S = \left[\pi \times (R_{OC}^2 - R_{IC}^2) \times h\right] / [2 \times \pi \times R_{OC} \times h] = 80.95$ mm, as depicted in Fig. 4. The measurement of free shrinkage by utilizing dial gauges with a precision of 10^{-3} mm was started at the age of 1.5 d after casting, and the net age, t_{net}, was defined as the elapsed time since that time (i.e. $t_{net} = t - 1.5$), as reported in [28].

2.4. Mechanical properties investigation

Mechanical properties tests were conducted on specimens at the same time to determine the elastic modulus and the strength of concrete according to Chinese Standard GB/T 50081-2002 [54]. Elastic modulus and strength were calculated by the average values of three concrete specimens. The cubic compressive strength at 28 d was 66.39, 69.16, 71.23, and 73.14 MPa, which increased by 4.17%, 7.29%, and 10.17% when the amount of double hooked-end steel fiber increased from 0% to 0.12%, 0.24%, and 0.36% for mixtures SF00, SF12, SF24, and SF36, respectively.

Splitting tensile strength was obtained by testing 150 mm cubic concrete specimens. The time-dependent splitting tensile strength is calculated by Eq. (1) [55].

$$f_{sp}(t) = f_{sp,28} \exp\left[S_1\left(1 - \sqrt{\frac{28}{t}}\right)\right] \quad (1)$$

in which $f_{sp}(t)$ = time-dependent splitting tensile strength of concrete, in MPa; $f_{sp,28}$ = splitting tensile strength of concrete at 28 d, in MPa; t = age of concrete after casting, in d; and S_1 = a fitting parameter.

The splitting tensile strength at 28 d was 3.66, 4.29, 4.74, and 4.95 MPa, which increased by 17.21%, 29.51%, and 35.25% when the amount of double hooked-end steel fiber increased from 0% to 0.12%, 0.24%, and 0.36% for mixtures SF00, SF12, SF24, and SF36, respectively. Results on strength were in accordance with that reported in [18,56]. Results reported in [18] indicate that the addition of steel fiber improves the compressive strength of concrete compared with plain concrete. Results reported in [56] indicate that the addition of steel fiber enhances the tensile strength of concrete.

The value of compressive elastic modulus was obtained by testing prismatic specimen with the size of 300 mm × 150 mm × 150 mm. The early-age tensile elastic modulus was considered to be almost equivalent to the early-age compressive elastic modulus in the present study, as reported in [51,57]. The time-dependent elastic modulus of concrete is calculated by Eq. (2) [58].

$$E_c(t) = E_{c,28} \exp\left[S_2\left(1 - \sqrt{\frac{28}{t}}\right)\right] \quad (2)$$

in which $E_c(t)$ =time-dependent elastic modulus of concrete, in GPa; $E_{c,28}$ = elastic modulus of concrete at 28 d, in GPa; and S_2 =a fitting parameter.

The elastic modulus at 28 d after casting was 51.60, 53.17, 58.08, and 60.42 GPa, which increased by 3.04%, 12.56%, and 17.09% when the amount of double hooked-end steel fiber increased from 0% to 0.12%, 0.24%, and 0.36% for mixtures SF00, SF12, SF24, and SF36, respectively. Table 2 depicts the results of time-dependent splitting tensile strength and time-dependent elastic modulus of HSC.

3. Results and discussion

3.1. Influence of double hooked-end steel fiber on steel ring strain

Fig. 5 depicts the relationship between steel ring strain and age of concrete ring specimens. A sharp decrease of steel ring strain

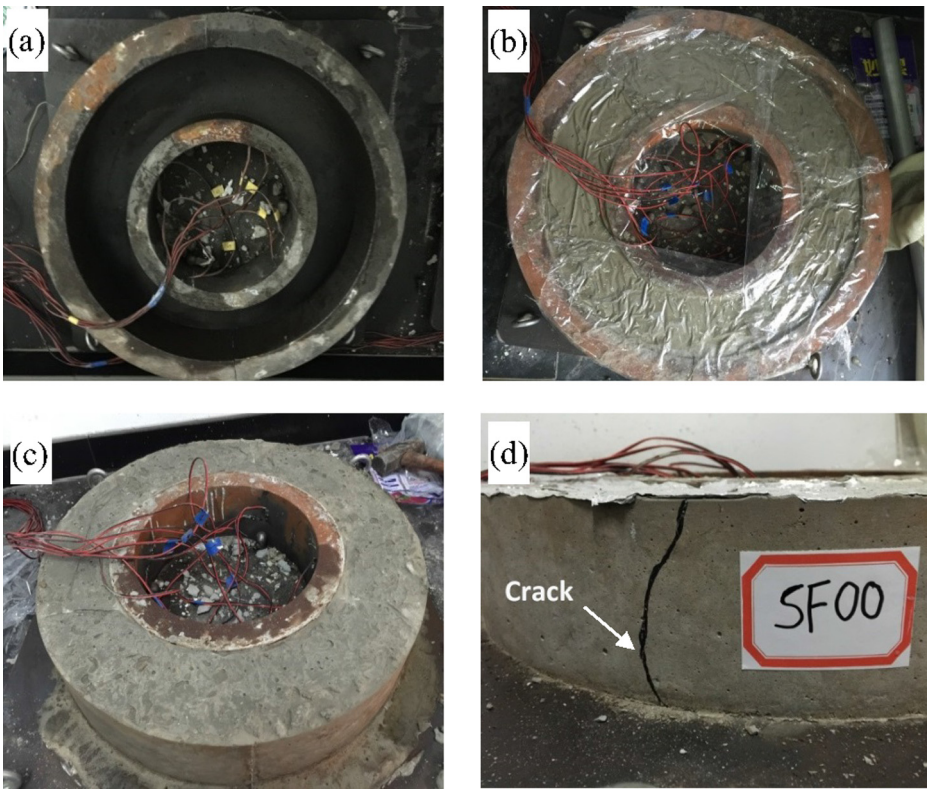

Fig. 3. Restrained ring test specimens: (a) Test set-up; (b) Placing concrete; (c) After demoulding; (d) Cracking.

represented the occurrence of cracking, as reported in [27]. A visible crack occurred in mixture SF00 at the age of 21.25 d after casting, no crack occurred for concrete ring specimens for mixtures SF12, SF24, and SF36 during the period of test, as depicted in Fig. 3 (d).

The steel ring strain decreased with increasing amount of double hooked-end steel fiber, as depicted in Fig. 5. At the age of 7 d after casting, the steel ring strain was −68, −51, −44, and −30 με, the absolute value of which decreased by 25.0%, 35.3%, and 55.9% when the amount of double hooked-end steel fiber increased from 0% to 0.12%, 0.24%, and 0.36% for mixtures SF00, SF12, SF24, and SF36, respectively. For mixtures SF12, SF24, and SF36, the increasing rates of steel ring strain were slower than that for mixture SF00, which indicated that the addition of double hooked-end steel fiber reduced the restrained shrinkage of concrete specimens, as reported in [39]. Results on shrinkage were in accordance with that reported in [37,38]. Results reported in [37] indicate that the cracking area of total plastic shrinkage decreases by nearly 40% for concrete with steel fiber volume fraction of 0.1% compared with plain concrete. Results reported in [38] indicate that the strain of shrinkage at 28 d decreases by 29% for concrete with steel fiber volume fraction of 0.2% compared with control concrete with no fiber.

3.2. Influence of double hooked-end steel fiber on residual stress of HSC

The shrinkage of concrete ring specimen was under restrained condition when the concrete dried, which induced tensile stress in the concrete specimen, as reported in [39]. The steel ring strain, ε_{st}, can be utilized to determine the development of residual tensile stress, $\sigma_{res.}(r)$, in the concrete ring [59]. The concrete and steel ring suffered interface pressures, $P_{res.}$, which were equivalent in value and in the opposite directions, as depicted in Fig. 2(c) and (d). The $\sigma_{res.}(r)$ reached maximum when $r = R_{OS}$ (i.e. at the interface between steel and concrete ring). The maximum residual tensile stress, $\sigma_{res.max}$, is calculated by Eq. (3) [26].

$$\sigma_{res.\max} = -\varepsilon_{st} \cdot E_S \cdot \frac{R_{OS}^2 - R_{IS}^2}{2R_{OS}^2} \cdot \frac{R_{OS}^2 + R_{OC}^2}{R_{OC}^2 - R_{OS}^2} \tag{3}$$

in which $\sigma_{res.max}$ = the maximum residual tensile stress, in MPa; ε_{st} = the steel ring strain, in με; E_S = the elastic modulus of steel ring, in GPa; R_{OS} = the radius of outer steel ring, in mm (162.5 mm); R_{IS} = the radius of inner steel ring, in mm (127.5 mm); and R_{OC} = the radius of inner steel ring, in mm (262.5 mm).

The maximum residual stress decreased with increasing amount of double hooked-end steel fiber, as depicted in Fig. 6. At the age of 21.25 d after casting, the maximum residual stress of concrete ring specimens was 3.17, 2.38, 2.07, and 1.62 MPa, which decreased by 24.9%, 34.7%, and 48.9% when the amount of double hooked-end steel fiber increased from 0% to 0.12%, 0.24%, and 0.36% for mixtures SF00, SF12, SF24, and SF36, respectively. Results on residual stress were in accordance with that reported in [60]. Results reported in [60] indicate that the residual stress decreases with increasing amount of steel fiber.

3.3. Influence of double hooked-end steel fiber on free shrinkage of HSC

Free shrinkage is a property of great importance relating to the durability of concrete [61]. The results were calculated by the average values of three prismatic specimens. The free shrinkage decreased with increasing amount of double hooked-end steel fiber, as depicted in Fig. 7. At the net age of 7 d, the free shrinkage was −232, −151, −107, and −68 με, the absolute value of which decreased by 34.9%, 53.9%, and 70.7% when the amount of double hooked-end steel fiber increased from 0% to 0.12%, 0.24%, and 0.36% for mixtures SF00, SF12, SF24, and SF36, respectively.

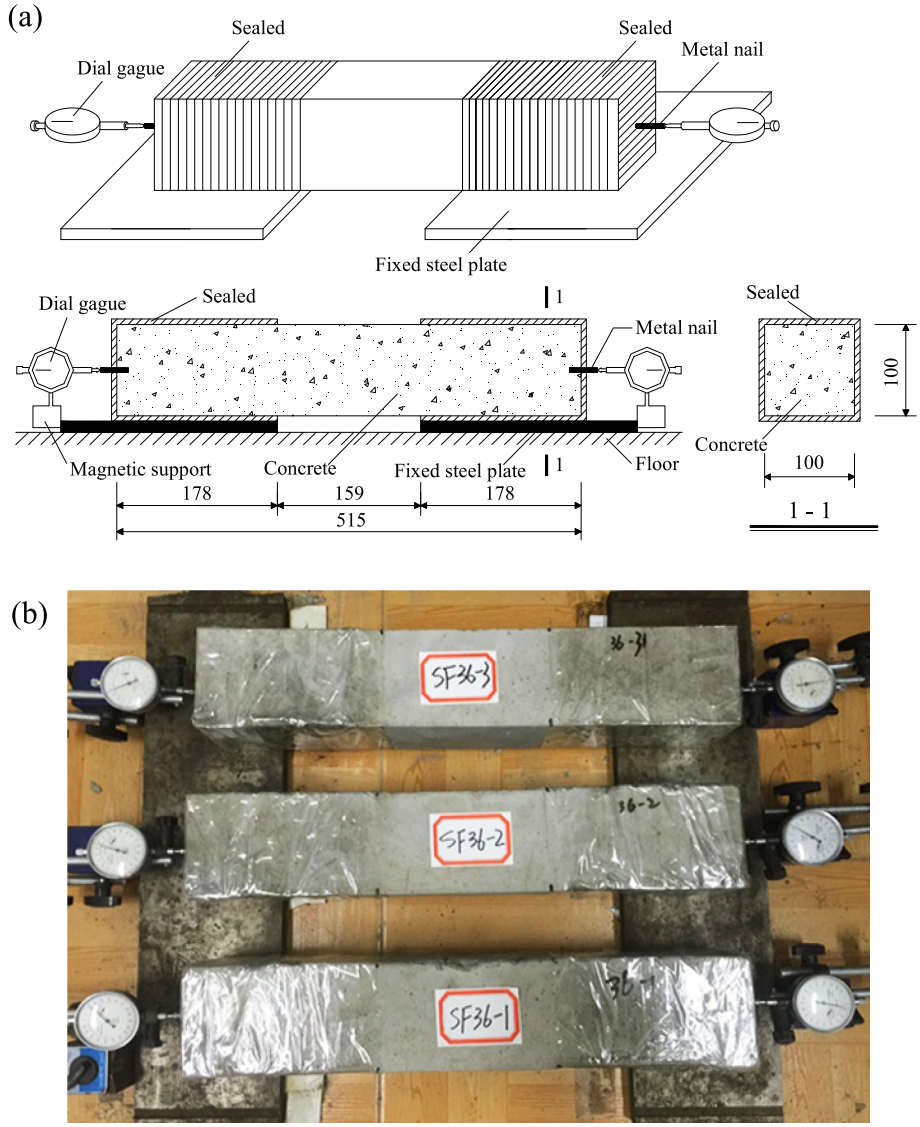

Fig. 4. Prismatic specimens with sealed ends for free shrinkage measurement: (a) Schematic drawing; (b) Photograph (all units in mm).

Table 2
Splitting tensile strength, elastic modulus and regression coefficients of all mixtures.

Concrete mixture	Splitting tensile strength (MPa)			S_1	R^2	Elastic modulus (GPa)			S_2	R^2
	3 d	7 d	28 d			3 d	7 d	28 d		
SF00	3.17	3.49	3.66	0.065	0.992	45.64	49.96	51.60	0.054	0.925
SF12	3.60	3.98	4.29	0.083	0.995	47.47	51.30	53.17	0.051	0.955
SF24	4.24	4.53	4.74	0.052	0.990	50.17	55.06	58.08	0.067	0.977
SF36	4.54	4.72	4.95	0.043	0.994	51.39	56.47	60.42	0.076	0.993

The amount of large pores in concrete specimens increases with increasing amount of steel fiber, which increases the toughness and decreases the capillary pressure of concrete specimens [37]. Therefore, the shrinkage resistance of concrete was influenced by the amount of double hooked-end steel fiber significantly. Results on shrinkage were in accordance with that reported in [32,62]. Results reported in [32] indicate that drying shrinkage decreases with increasing amount of steel fiber. Results reported in [62] indicate that the addition of steel fiber reduces the autogenous shrinkage of plain concrete.

3.4. Influence of double hooked-end steel fiber on stress rate of HSC

Cracking potential is usually described by stress rate, which is an important element to control the cracking age [51]. Eq. (4) is utilized to calculate the stress rate, S, of concrete ring specimens [30,63].

$$S = \frac{G|\alpha|}{2\sqrt{t_r}} \tag{4}$$

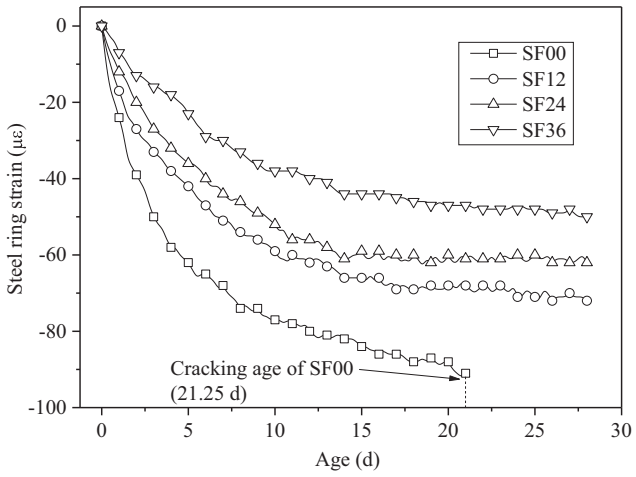

Fig. 5. Relationship between steel ring strain and age.

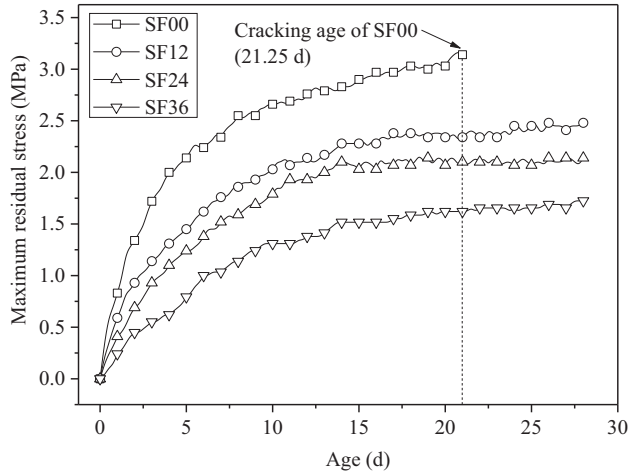

Fig. 6. Relationship between maximum residual stress in concrete ring specimens and age.

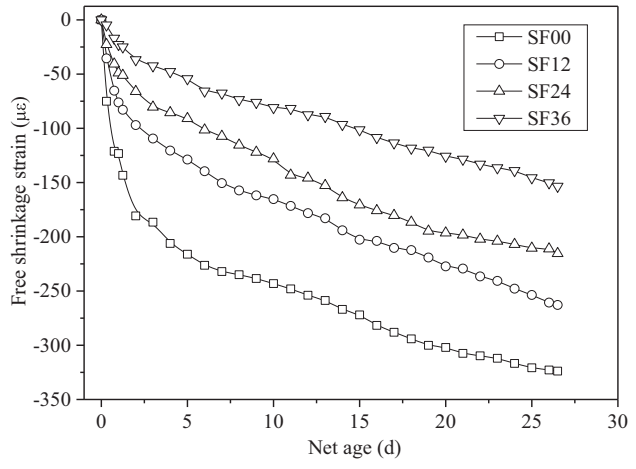

Fig. 7. Relationship between free shrinkage and net age.

in which S = the stress rate of concrete ring specimens, in MPa/d; G = a constant determined by the dimensions of ring setup, in GPa; α = strain rate factor for strain gauges, in με/d$^{1/2}$; and t_r = the elapsed time from 1.5 d to the cracking age or the elapsed time from 1.5 d to the end of ring test, in d.

Eq. (5) is utilized to calculate G [63].

$$G = \frac{E_s R_{IC} h_s}{R_{IS} h_c} \tag{5}$$

in which R_{IC} = radius of inner concrete ring, in mm (162.5 mm); h_s = thickness of steel ring, in mm (35 mm); and h_c =thickness of concrete ring, in mm (100 mm).

Eq. (6) is utilized to calculate α [30,63].

$$\varepsilon_{net}(t) = \alpha\sqrt{t_{net}} + k \tag{6}$$

in which $\varepsilon_{net}(t)$ = the net steel ring strain calculated as the differential value of the steel ring strain at any recorded time and that at the age of 1.5 d after casting, in με; t_{net} = the net age, in d; and k = a regression constant. The strain rate factor α was determined with the linear regression analysis results about the net steel ring strain and the square root of net age, as depicted in Fig. 8. The results of α were −12.893, −9.833, −9.302, and −8.571 με/d$^{1/2}$ with the R^2 values of 0.968, 0.922, 0.869, and 0.939 for mixtures SF00, SF12, SF24, and SF36, respectively.

For mixture SF00, the occurrence of crack was at the net age of 19.75 d. For mixtures SF12, SF24, and SF36, no crack occurred during the whole test. The stress rate decreased with increasing amount of double hooked-end steel fiber, as depicted in Fig. 9. At the net age of 7 d, the stress rate of specimens was 0.141, 0.108, 0.102, and 0.094 MPa/d, which decreased by 23.4%, 27.7%, and 33.3% when the amount of double hooked-end steel fiber increased from 0% to 0.12%, 0.24%, and 0.36% for mixtures SF00, SF12, SF24, and SF36, respectively. Cracking potential of concrete can be classified into 4 levels in Table 3 depending on cracking time and stress rate according to ASTM C1581 [30], as reported in [63]. Mixture SF00 belonged to 'Moderate-Low' level; mixtures SF12, SF24, and SF36 belonged to 'Low' level in the present study. Therefore, the concrete with more amount of double hooked-end steel fiber showed lower cracking potential.

3.5. Influence of double hooked-end steel fiber on stress relaxation of HSC

Relaxed stress is calculated as the differential value between theoretical elastic stress and residual stress [28,39]. The self-restraint and the restraint caused by steel ring are important factors to determine the residual stress in concrete ring specimens [26]. The concrete ring specimens are assumed to be under complete restrained condition considering that steel rings are rigid [64]. However, steel rings are not rigid enough in practice, which

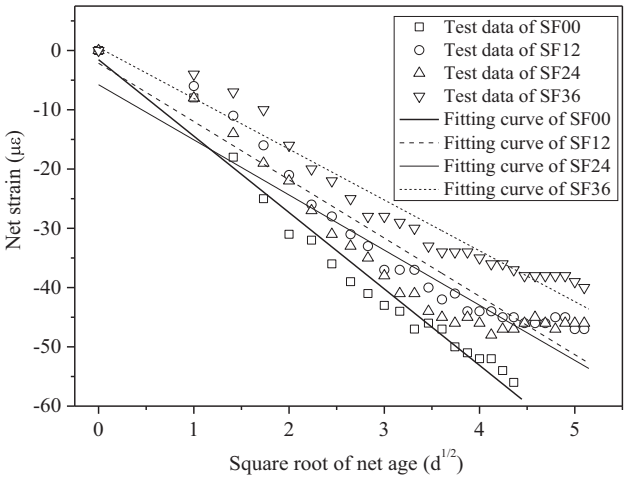

Fig. 8. Relationship between net strain and square root of net age.

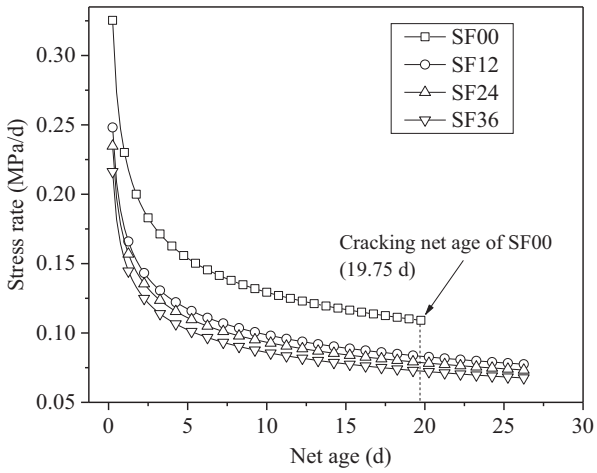

Fig. 9. Relationship between stress rate and net age.

Table 3
Classification of cracking potential [30].

Net time to cracking,t_{cr} (d)	Stress rate, S(MPa/d)	Cracking potential
$0 < t_{cr} \leqslant 7$	$S \geqslant 0.34$	High
$7 < t_{cr} \leqslant 14$	$0.17 \leqslant S < 0.34$	Moderate-High
$14 < t_{cr} \leqslant 28$	$0.10 \leqslant S < 0.17$	Moderate-Low
$t_{cr} > 28$	$S < 0.10$	Low

leads to deformation of steel rings when they are under the load caused by shrinkage [65].

Eq. (7) is utilized to determine the value of radial deformation, ΔU_{sh}, assuming that the concrete ring deformed without restraint [26,65].

$$\Delta U_{sh} = R_{IC}\Delta\varepsilon_{sh} \tag{7}$$

in which ΔU_{sh} =the value of radial deformation, in mm; and $\Delta\varepsilon_{sh}$ = incremental free shrinkage strain, in με.

A fictitious pressure, ΔP_{el}, is assumed to exist on the interface between the steel ring and concrete ring [30,66]. Eqs. (8) and (9) are utilized to determine the displacement of the interface between the steel ring and concrete ring, respectively [26,65].

$$U_{st} = -\Delta P_{el}\left(\frac{R_{OS}^2\left[(1+\upsilon_s)R_{IS}^2 + (1-\upsilon_s)R_{OS}^2\right]}{E_s R_{OS}\left(R_{OS}^2 - R_{IS}^2\right)}\right) \tag{8}$$

$$U_c = \Delta P_{el}\left(\frac{R_{IC}^2\left[(1+\upsilon_c)R_{OC}^2 + (1-\upsilon_c)R_{IC}^2\right]}{E_c R_{IC}\left(R_{OC}^2 - R_{IC}^2\right)}\right) \tag{9}$$

in which U_{st} = displacement of outer surface of steel ring, in mm; U_c =displacement of the inner surface of concrete ring, in mm; ΔP_{el} = a fictitious pressure, in MPa; E_c = time-dependent elastic modulus of concrete, in GPa; υ_c = Poisson's ratio of concrete; and υ_s = Poisson's ratio of inner steel ring.

The value of radial deformation, ΔU_{sh}, and the differential value of two displacements should be equivalent, which is given by Eq. (10) [26,65].

$$U_{st} - U_c = \Delta U_{sh} \tag{10}$$

Eq. (11) is obtained by substituting Eqs. (7) – (9) into Eq.(10) [22,68]:

$$\Delta P_{el} = -\frac{\Delta\varepsilon_{sh}E_c}{\frac{E_c}{E_s}\frac{\left[(1+\upsilon_s)R_{IS}^2+(1-\upsilon_s)R_{OS}^2\right]}{R_{OS}^2-R_{IS}^2} + \frac{\left[(1+\upsilon_c)R_{OC}^2+(1-\upsilon_c)R_{IC}^2\right]}{R_{OC}^2-R_{IC}^2}} \tag{11}$$

Eq. (12) is utilized to determine the incremental circumferential theoretical elastic stress of concrete specimens, $\Delta\sigma_{el}(r)$, with the result in Eq. (12) [26,65].

$$\Delta\sigma_{el}(r) = \Delta P_{el}\frac{R_{OS}^2}{R_{OC}^2 - R_{OS}^2}\left(1 + \frac{R_{OC}^2}{r^2}\right) \tag{12}$$

in which $\Delta\sigma_{el}(r)$ = the incremental circumferential theoretical elastic stress of concrete specimens, in MPa; and r = radius of concrete ring between 162.5 and 262.5 mm, in mm.

Eq. (12) reaches the maximum on the contact surface of the steel ring and concrete ring when $r = R_{OS}$. Eq. (13) is utilized to determine incremental maximum theoretical elastic stress, which is simplified by substituting the dimensions of specimens into Eq. (12).

$$\Delta\sigma_{el,\max} = -\frac{2.24\Delta\varepsilon_{sh}E_c}{3.93\frac{E_c}{E_s} + 2.44} \tag{13}$$

in which $\Delta\sigma_{el,\max}$ = incremental maximum theoretical elastic stress, in MPa. The relationship between incremental maximum theoretical elastic stress and net age is depicted in Fig. 10.

Eq. (14) is utilized to determine the incremental creep-related relaxed stress, $\Delta\sigma_{rel}$, which is induced by creep in the concrete ring specimens, by calculating the differential value between the incremental maximum theoretical elastic stress, $\Delta\sigma_{el,\max}$, and the incremental maximum residual stress, $\Delta\sigma_{res,\max}$ [26,67].

$$\Delta\sigma_{rel} = \Delta\sigma_{el,\max} - \Delta\sigma_{res,\max} \tag{14}$$

in which $\Delta\sigma_{rel}$ = incremental relaxed stress, in MPa; and $\Delta\sigma_{res,\max}$ = incremental maximum residual stress, in MPa. The incremental maximum theoretical elastic stress and incremental maximum residual stress for different mixtures at net age are depicted in Fig. 11. The relaxed stress decreased with increasing amount of double hooked-end steel fiber, as depicted in Fig. 12. At the net age of 7 d, the relaxed stress in concrete ring specimens was 3.93, 2.41, 1.44, and 0.78 MPa, which decreased by 38.7%, 63.4%, and 80.2% when the amount of double hooked-end steel fiber increased from 0% to 0.12%, 0.24%, and 0.36% for mixtures SF00, SF12, SF24, and SF36, respectively.

3.6. Influence of double hooked-end steel fiber on cracking potential of HSC

The time-dependent cracking potential parameter, $\varphi_{CR}(t)$, is defined as the ratio of time-dependent maximum residual stress

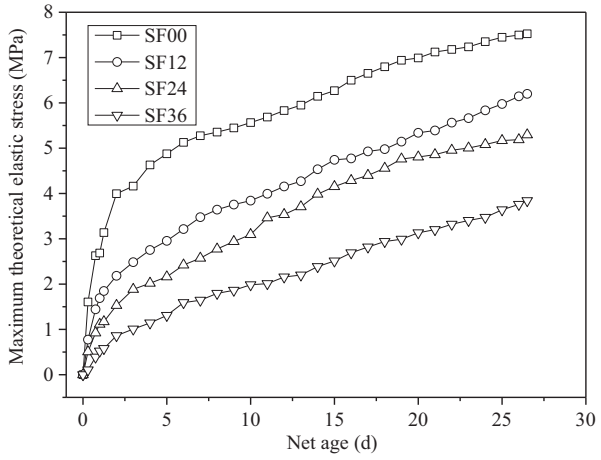

Fig. 10. Relationship between incremental maximum theoretical elastic stress and net age.

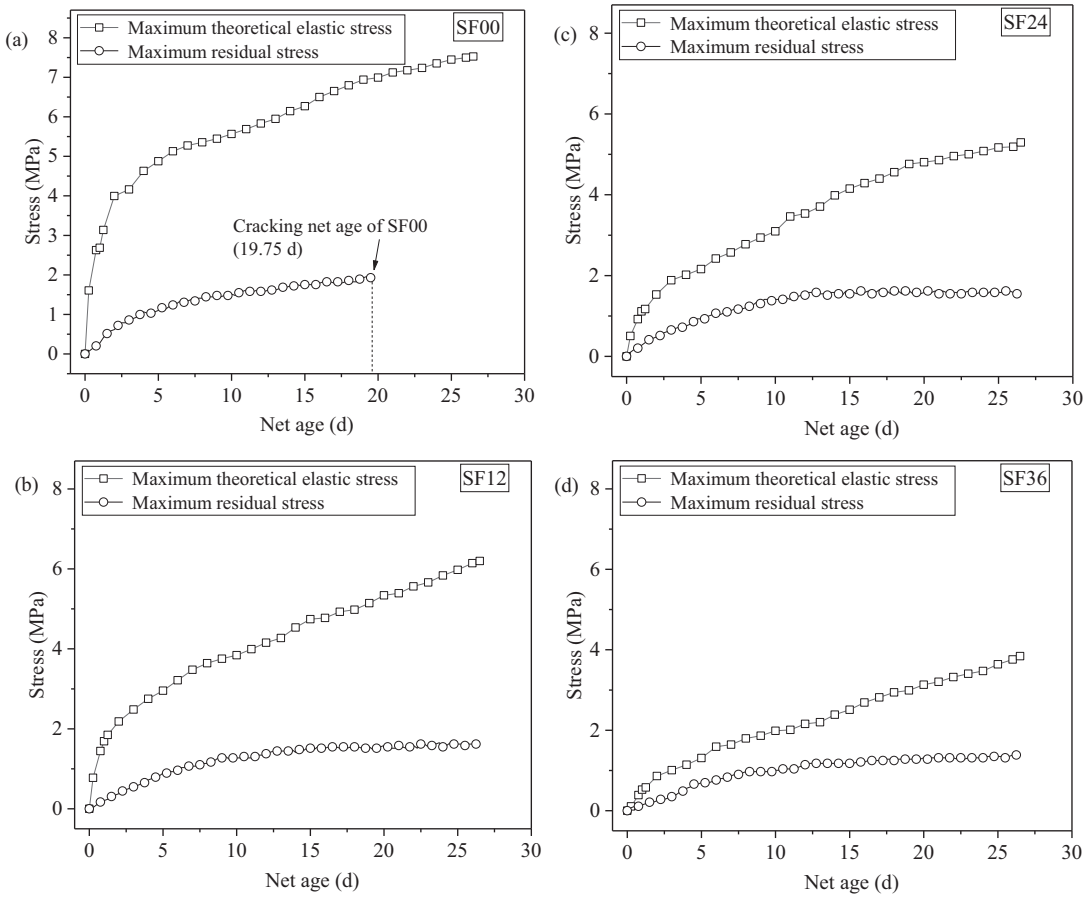

Fig. 11. Comparison on incremental maximum theoretical elastic stress and incremental maximum residual stress for different mixtures: (a) SF00; (b) SF12; (c) SF24; (d) SF36.

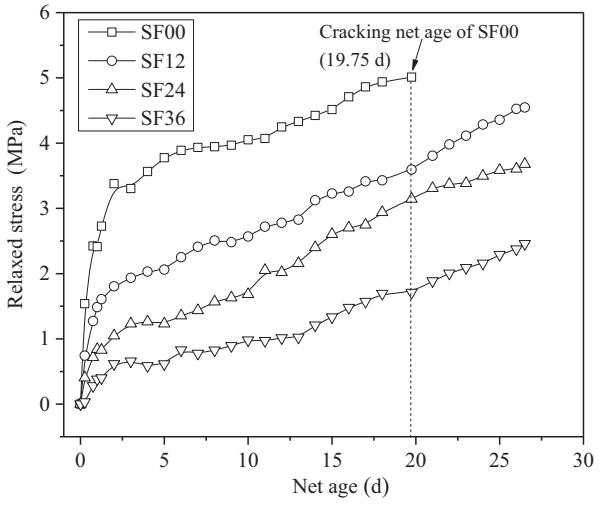

Fig. 12. Relationship between relaxed stress and net age.

to time-dependent splitting tensile strength, as given in Eq. (15) [26,67]. Fig. 13 depicts the relationship between residual stress or the splitting tensile strength and age for different mixtures.

$$\varphi_{CR}(t) = \frac{\sigma_{res,\max}(t)}{f_{sp}(t)} \tag{15}$$

in which $\varphi_{CR}(t)$ = cracking potential parameter.

The cracking potential of concrete ring specimens decreased with increasing amount of double hooked-end steel fiber, as depicted in Fig. 14. Cracking potential parameter at the age of 21.25 d after casting was 0.875, 0.561, 0.440, and 0.329, which decreased by 35.9%, 49.7%, and 62.4% when the amount of double hooked-end steel fiber increased from 0% to 0.12%, 0.24%, and 0.36% for mixtures SF00, SF12, SF24, and SF36, respectively. The crack occurs when $\varphi_{CR} = 1$ in theory, however, crack will occur when φ_{CR} is lower than 1 in practice [26,67]. Crack occurs even tensile stress is lower than tensile strength when concrete is under continuous stress due to creep failure [68]. Results on cracking potential were in accordance with that reported in [17]. Results reported in [17] indicate that the cracking potential decreases with increasing amount of steel fiber.

4. Conclusions

The investigations on influence of double hooked-end steel fiber on the behavior and cracking potential of HSC at early age utilizing ring test were conducted in the present study. The analysis was shown based on the results of the ring test, including steel ring strain, residual stress, relaxed stress, free shrinkage, stress rate and cracking potential of four HSC mixtures. The conclusions generalized from the experimental results were as follows:

(1) The steel ring strain decreased with increasing amount of double hooked-end steel fiber. The steel ring strain at the age of 7 d after casting was −68, −51, −44, and −30 με,

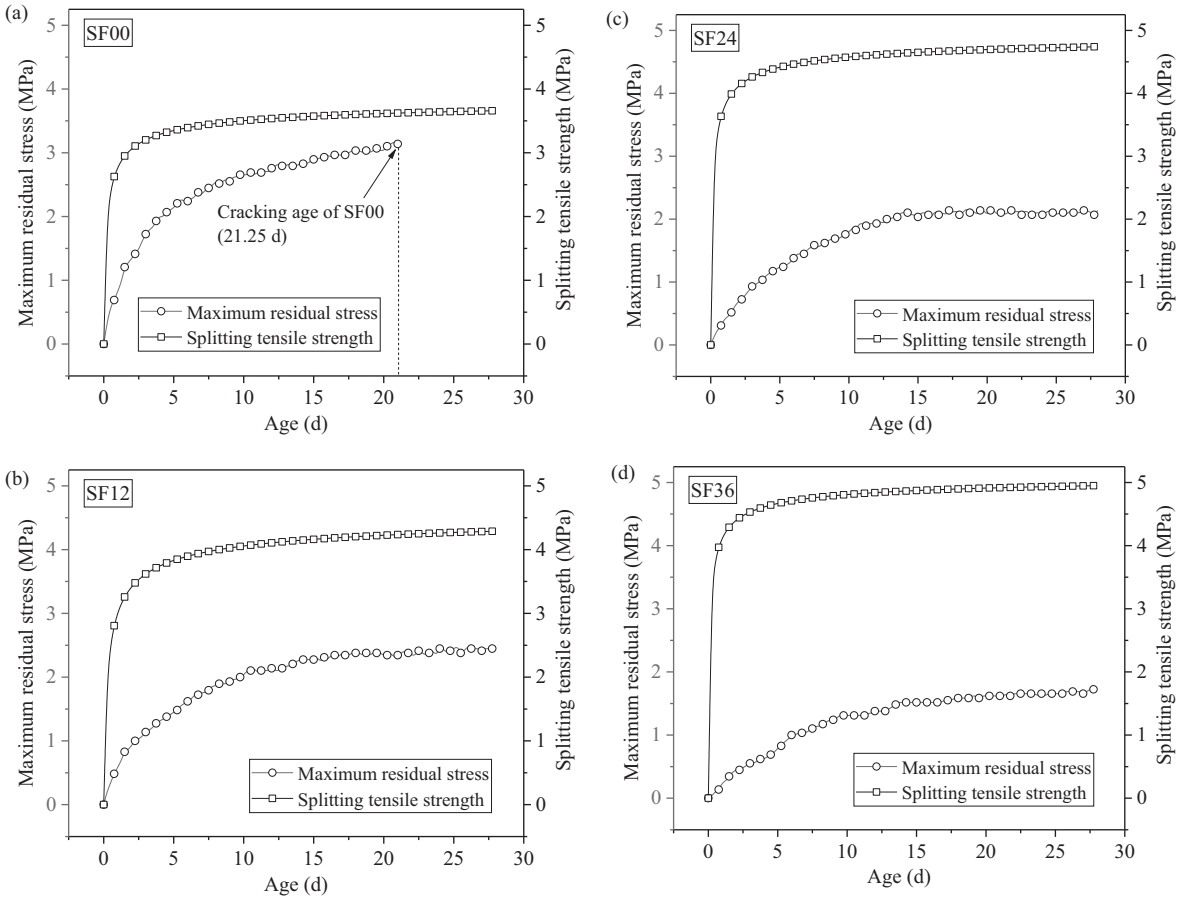

Fig. 13. Comparison on maximum residual stress and splitting tensile strength for different mixtures: (a) SF00; (b) SF12; (c) SF24; (d) SF36.

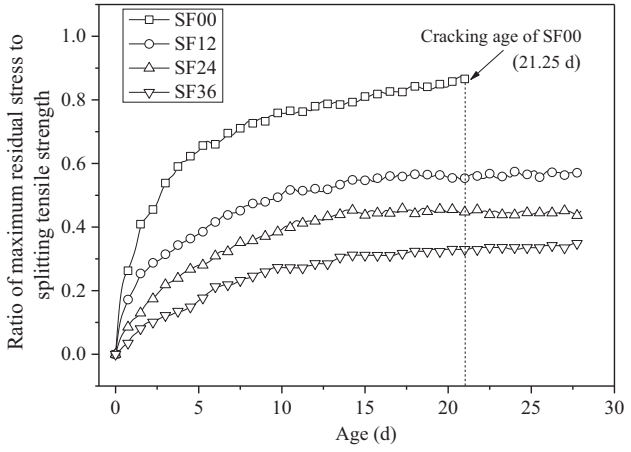

Fig. 14. Relationship between ratio of maximum residual stress to splitting tensile strength and age.

the absolute value of which decreased by 25.0%, 35.3%, and 55.9% when the amount of double hooked-end steel fiber increased from 0% to 0.12%, 0.24%, and 0.36%, respectively.

(2) The residual stress or relaxed stress decreased with increasing amount of double hooked-end steel fiber. The maximum residual stress at the age of 21.25 d after casting or relaxed stress at the net age of 7 d of concrete ring specimens was 3.17, 2.38, 2.07, and 1.62 MPa or 3.93, 2.41, 1.44, and 0.78 MPa, which decreased by 24.9%, 34.7%, and 48.9% or 38.7%, 63.4%, and 80.2% when the amount of double hooked-end steel fiber increased from 0% to 0.12%, 0.24%, and 0.36%, respectively.

(3) The free shrinkage or stress rate decreased with increasing amount of double hooked-end steel fiber. The free shrinkage strain or stress rate at the net age of 7 d was −232, −151, −107, and −68 με or 0.141, 0.108, 0.102, and 0.094 MPa/d, the absolute value of which decreased by 34.9%, 53.9%, and 70.7% or by 23.4%, 27.7%, and 33.3% when the amount of double hooked-end steel fiber increased from 0% to 0.12%, 0.24%, and 0.36%, respectively.

(4) The cracking potential decreased with increasing amount of double hooked-end steel fiber. At the age of 21.25 d after casting, the cracking potential parameter was 0.875, 0.561, 0.440, and 0.329, which decreased by 35.9%, 49.7%, and 62.4% when the amount of double hooked-end steel fiber increased from 0% to 0.12%, 0.24%, and 0.36%, respectively.

Declaration of Competing Interest

The authors declare that they have no known competing financial interests or personal relationships that could have appeared to influence the work reported in this paper.

Acknowledgements

The financial support of the National Natural Science Foundation of China (Grant No. 51879092) is gratefully acknowledged. Present work is also sponsored by Qing Lan Project of Jiangsu

Province. The support of the Fundamental Research Funds for Central Universities (Grant No. 2017B41114) is also gratefully acknowledged.

References

[1] D.J. Shen, W.T. Wang, J.W. Liu, X.G. Zhao, G.Q. Jiang, Influence of Barchip fiber on early-age cracking potential of high performance concrete under restrained condition, Constr. Build. Mater. 187 (2018) 118–130.

[2] A. Poursaee, C.M. Hansson, The influence of longitudinal cracks on the corrosion protection afforded reinforcing steel in high performance concrete, Cem. Concr. Res. 38 (8–9) (2008) 1098–1105.

[3] R. Bleszynski, R.D. Hooton, M.D. Thomas, C.A. Rogers, Durability of ternary blend concrete with silica fume and blast-furnace slag: laboratory and outdoor exposure site studies, Mater. J. 99 (5) (2002) 499–508.

[4] K. Kovler, S. Igarashi, A. Bentur, Tensile creep behavior of high strength concretes at early ages, Mater. Struct. 32 (5) (1999) 383–387.

[5] R. Khatri, V. Sirivivatnanon, W. Gross, Effect of different supplementary cementitious materials on mechanical properties of high performance concrete, Cem. Concr. Res. 25 (1) (1995) 209–220.

[6] D.J. Shen, C. Liu, C.C. Li, X.G. Zhao, G.Q. Jiang, Influence of Barchip fiber length on early-age behavior and cracking resistance of concrete internally cured with super absorbent polymers, Constr. Build. Mater. 214 (2019) 219–231.

[7] D.P. Bentz, K.A. Snyder, Protected paste volume in concrete: Extension to internal curing using saturated lightweight fine aggregate, Cem. Concr. Res. 29 (11) (1999) 1863–1867.

[8] D. Cusson, T. Hoogeveen, An experimental approach for the analysis of early-age behaviour of high-performance concrete structures under restrained shrinkage, Cem. Concr. Res. 37 (2) (2007) 200–209.

[9] D.J. Shen, B.Z. Zhou, M.L. Wang, Y. Chen, G.Q. Jiang, Predicting relative humidity of early-age concrete under sealed and unsealed conditions, Mag. Concr. Res. (2018), https://doi.org/10.1680/jmacr.18.00068.

[10] T. Voigt, G. Ye, Z. Sun, S.P. Shah, K. Van Breugel, Early age microstructure of Portland cement mortar investigated by ultrasonic shear waves and numerical simulation, Cem. Concr. Res. 35 (5) (2005) 858–866.

[11] K. Wang, D.C. Jansen, S.P. Shah, A.F. Karr, Permeability study of cracked concrete, Cem. Concr. Res. 27 (3) (1997) 381–393.

[12] G. Yuan, J. Zhang, P. Han, Determination of stress relaxation parameters of concrete in tension at early-age by ring test, Constr. Build. Mater. 41 (2) (2013) 152–164.

[13] D.J. Shen, Q. Yang, C.B. Huang, Z.H. Cui, J.Y. Zhang, Tests on seismic performance of corroded reinforced concrete shear walls repaired with basalt fiber-reinforced polymers, Constr. Build. Mater. 209 (2019) 508–521.

[14] V. Afroughsabet, L. Biolzi, T. Ozbakkaloglu, High-performance fiber-reinforced concrete: a review, J. Mater. Sci. 51 (14) (2016) 6517–6551.

[15] V. Afroughsabet, T. Ozbakkaloglu, Mechanical and durability properties of high-strength concrete containing steel and polypropylene fibers, Constr. Build. Mater. 94 (2015) 73–82.

[16] A. Gholampour, T. Ozbakkaloglu, Fiber-reinforced concrete containing ultra high-strength micro steel fibers under active confinement, Constr. Build. Mater. 187 (2018) 299–306.

[17] D.J. Shen, X.Z. Liu, Q.Y. Li, L. Sun, W.T. Wang, Early-age behavior and cracking resistance of high-strength concrete reinforced with Dramix 3D steel fiber, Constr. Build. Mater. 196 (2019) 307–316.

[18] S. Eswari, P.N. Raghunath, K. Suguna, Ductility performance of concrete with Dramix steel micro-reinforcement, Adv. Nat. Appl. Sci. 2 (3) (2008) 243–248.

[19] V. Afroughsabet, L. Biolzi, T. Ozbakkaloglu, Influence of double hooked-end steel fibers and slag on mechanical and durability properties of high performance recycled aggregate concrete, Compos. Struct. 181 (2017) 273–284.

[20] S. Abdallah, M. Fan, D.W. Rees, Analysis and modelling of mechanical anchorage of 4D/5D hooked end steel fibres, Mater. Des. 112 (2016) 539–552.

[21] S. Abdallah, M. Fan, X. Zhou, S.L. Geyt, Anchorage effects of various steel fibre architectures for concrete reinforcement, Int. J. Concr. Struct. Mater. 10 (3) (2016) 325–335.

[22] P.S. Song, S. Hwang, Mechanical properties of high-strength steel fiber-reinforced concrete, Constr. Build. Mater. 18 (9) (2004) 669–673.

[23] M.F. Cyr, C. Ouyang, S.P. Shah, Design of hybrid-fiber reinforcement for shrinkage cracking by crack width prediction, Brittle Matrix Compos (2003) 243–252.

[24] E.T. Dawood, M. Ramli, Development of high strength flowable mortar with hybrid fiber, Constr. Build. Mater. 24 (6) (2010) 1043–1050.

[25] S.P. Shah, M.E. Karaguler, M. Sarigaphuti, Effects of shrinkage-reducing admixtures on restrained shrinkage cracking of concrete, ACI Mater. J. 89 (3) (1992) 289–295.

[26] A.B. Hossain, J. Weiss, Assessing residual stress development and stress relaxation in restrained concrete ring specimens, Cem. Concr. Compos. 26 (5) (2004) 531–540.

[27] J.H. Moon, J. Weiss, Estimating residual stress in the restrained ring test under circumferential drying, Cem. Concr. Compos. 28 (5) (2006) 486–496.

[28] D.J. Shen, K.Q. Liu, C.Y. Wen, Y.Q. Shen, G.Q. Jiang, Early-age cracking resistance of ground granulated blast furnace slag concrete, Constr. Build. Mater. 222 (2019) 278–287.

[29] I. Khan, A. Castel, R.I. Gilbert, Tensile creep and early-age concrete cracking due to restrained shrinkage, Constr. Build. Mater. 149 (2017) 705–715.

[30] ASTM C1581 / C1581M–18a, Standard Test Method for Determining Age at Cracking and Induced Tensile Stress Characteristics of Mortar and Concrete under Restrained Shrinkage, ASTM International, West Conshohocken, PA, 2018.

[31] S. Aashto, Standard practice for estimating the cracking tendency of concrete, AASHTO Designation (1996) 34–99.

[32] S. Zhao, C. Li, M. Zhao, X. Zhang, Experimental study on autogenous and drying shrinkage of steel fiber reinforced lightweight-aggregate concrete, Adv. Mater. Sci. Eng. 2016 (6) (2016) 1–9.

[33] D.J. Shen, C. Liu, Z.Z. Feng, S.S. Zhu, C. Liang, Influence of ground granulated blast furnace slag on the early-age anti-cracking property of internally cured concrete, Constr. Build. Mater. 223 (2019) 233–243.

[34] S.H. Kwon, S.P. Shah, Prediction of early-age cracking of fiber-reinforced concrete due to restrained shrinkage, ACI Mater. J. 105 (4) (2008) 381–389.

[35] K. Kiviste, A. Ryabchikov, H. Lille, Determination of shrinkage of fibre reinforced concrete, Civ. Eng. 11 (2011) 113–116.

[36] D.J. Shen, W.T. Wang, Q.Y. Li, P.P. Yao, G.Q. Jiang, Early-age behaviour and cracking potential of fly ash concrete under restrained condition, Mag. Concr. Res. (2018), https://doi.org/10.1680/jmacr.18.00106.

[37] K. Wang, S.P. Shah, P. Phuaksuk, Plastic shrinkage cracking in concrete materials-influence of fly ash and fibers, Mater. J. 98 (6) (2001) 458–464.

[38] N. Yousefieh, A. Joshaghani, E. Hajibandeh, M. Shekarchi, Influence of fibers on drying shrinkage in restrained concrete, Constr. Build. Mater. 148 (2017) 833–845.

[39] D.J. Shen, K.Q. Liu, Y. Ji, H.F. Shi, J.Y. Zhang, Early-age residual stress and stress relaxation of high-performance concrete containing fly ash, Mag. Concr. Res. 70 (14) (2017) 726–738.

[40] K. Raoufi, J. Schlitter, D. Bentz, J. Weiss, Parametric assessment of stress development and cracking in internally cured restrained mortars experiencing autogenous deformations and thermal loading, Adv. Civ. Eng. (2011) 1–16.

[41] Y. Wei, W. Hansen, Tensile creep behavior of concrete subject to constant restraint at very early ages, J. Mater. Civ. Eng. 25 (9) (2012) 1277–1284.

[42] S.A. Altoubat, D.A. Lange, Creep, shrinkage, and cracking of restrained concrete at early age, ACI Mater. J. 98 (4) (2001) 323–331.

[43] E. García-Taengua, S. Arango, J.R. Martí-Vargas, P. Serna, Flexural creep of steel fiber reinforced concrete in the cracked state, Constr. Build. Mater. 65 (2014) 321–329.

[44] R. Olivito, F. Zuccarello, An experimental study on the tensile strength of steel fiber reinforced concrete, Compos. B Eng. 41 (3) (2010) 246–255.

[45] M. Nataraja, N. Dhang, A. Gupta, Stress–strain curves for steel-fiber reinforced concrete under compression, Cem. Concr. Compos. 21 (5–6) (1999) 383–390.

[46] Z.L. Wang, Y.S. Liu, R. Shen, Stress–strain relationship of steel fiber-reinforced concrete under dynamic compression, Constr. Build. Mater. 22 (5) (2008) 811–819.

[47] A.R. Khaloo, N. Kim, Mechanical properties of normal to high-strength steel fiber-reinforced concrete, Cem. Concr. Aggregates 18 (2) (1996) 92–97.

[48] K. Marar, Ö. Eren, T. Celik, Relationship between impact energy and compression toughness energy of high-strength fiber-reinforced concrete, Mater. Lett. 47 (4–5) (2001) 297–304.

[49] Chinese Standard, Common Portlad Cement GB 175–2007/XGI-2009, Ministry of Construction, China, 2009 (in Chinese).

[50] ASTM / C150M–19a, Standard Specification for Portland Cement, ASTM International, West Conshohocken, PA, 2019.

[51] H.T. See, E.K. Attiogbe, M.A. Miltenberger, Shrinkage cracking characteristics of concrete using ring specimens, Mater. J. 100 (3) (2003) 239–245.

[52] Chinese Standard, Standard for Test Methods of Long-term Performance and Durability of Ordinary Concrete GB/T50082-2009, China Architecture and Building Press, China, 2009 (in Chinese).

[53] M. Grzybowski, S.P. Shah, Shrinkage cracking of fiber reinforced concrete, ACI Mater. J. 87 (2) (1990) 138–148.

[54] Chinese Standard, Test Method of Mechanical Properties on Ordinary Concrete GB/T 50081–2002, Ministry of Construction, China, 2002 (in Chinese).

[55] Eurocode 2, Design of Concrete Structures – Part 1–1: General Rules and Rules for Buildings, CEN (2004).

[56] F.A. Olutoge, V. Bhashya, G. Ramesh, B. Hanumantharai, S.S. Kumar, Evaluation of residual strength properties of steel fiber reinforced concrete, J. Emerging Trends Eng. Appl. Sci. 4 (2) (2013) 168–172.

[57] T. Wee, H. Lu, S. Swaddiwudhipong, Tensile strain capacity of concrete under various states of stress, Mag. Concr. Res. 52 (3) (2000) 185–193.

[58] CEB-FIP, fib model code for concrete structures 2010, Bulletin Information No. 199, comtie European du Béton/Fédération International de laPrecontrainte, Lausanne, 2013.

[59] D.J. Shen, H.F. Shi, X.J. Tang, Y. Ji, G.Q. Jiang, Effect of internal curing with super absorbent polymers on residual stress development and stress relaxation in restrained concrete ring specimens, Constr. Build. Mater. 120 (2016) 309–320.

[60] H.R. Shah, J. Weiss, Quantifying shrinkage cracking in fiber reinforced concrete using the ring test, Mater. Struct. 39 (9) (2006) 887.

[61] W. Sun, H. Chen, X. Luo, H. Qian, The effect of hybrid fibers and expansive agent on the shrinkage and permeability of high-performance concrete, Cem. Concr. Res. 31 (4) (2001) 595–601.

[62] D. Saje, B. Bandelj, J. Šušteršic, J. Lopatic, F. Saje, Autogenous and drying shrinkage of fibre reinforced high-performance concrete, J. Adv. Concr. Technol. 10 (2) (2012) 59–73.

[63] H.T. See, E.K. Attiogbe, M.A. Miltenberger, Potential for restrained shrinkage cracking of concrete and mortar, Cem. Concr. Aggregates 26 (2) (2004) 1–8.
[64] W.J. Weiss, W. Yang, S.P. Shah, Influence of specimen size/geometry on shrinkage cracking of rings, J. Eng. Mech. 126 (1) (2000) 93–101.
[65] D.Y. Yoo, J.J. Park, S.W. Kim, Y.S. Yoon, Influence of ring size on the restrained shrinkage behavior of ultra high performance fiber reinforced concrete, Mater. Struct. 47 (7) (2014) 1161–1174.
[66] D.Y. Yoo, J.J. Park, S.W. Kim, Y.S. Yoon, Early age setting, shrinkage and tensile characteristics of ultra high performance fiber reinforced concrete, Constr. Build. Mater. 41 (2013) 427–438.
[67] A.B. Hossain, A. Fonseka, H. Bullock, Early age stress development, relaxation, and cracking in restrained low W/B ultrafine fly ash mortars, J. Adv. Concr. Technol. 6 (2) (2008) 261–271.
[68] F. Wittmann, P. Roelfstra, H. Mihashi, Y.Y. Huang, X.H. Zhang, N. Nomura, Influence of age of loading, water-cement ratio and rate of loading on fracture energy of concrete, Mater. Struct. 20 (2) (1987) 103–110.